Geophysical Research Letters

RESEARCH LETTER
10.1029/2020GL089808

Dominant Process for Northward Propagation of Boreal Summer Intraseasonal Oscillation Over the Western North Pacific

Young-Min Yang[1], June-Yi Lee[2,3], and Bin Wang[1,4]

[1]Key Laboratory of Meteorological Disaster, Ministry of Education/International Joint Research Laboratory on Climate and Environment Change/Collaborative Innovation Center on Forecast and Evaluation of Meteorological Disasters, Nanjing University of Information Science and Technology, Nanjing, China, [2]Research Center for Climate Sciences and Department of Climate System, Pusan National University, Busan, South Korea, [3]Center for Climate Physics, Institute for Basic Science (IBS), Busan, South Korea, [4]Department of Atmosphere Science and International Pacific Research Center, University of Hawaii, Honolulu, HI, USA

Abstract Northward propagation of boreal summer intraseasonal oscillation (BSISO) over the Western North Pacific (WNP) has significant impacts on extreme events over Asia and Europe. Here we test hypotheses that northward propagation mechanisms over the WNP may differ from those over the Indian Ocean (IO) by performing numerical experiments with changing mean states through lowering the Tibetan Plateau (TP). Our results suggest that air-sea interaction plays a dominant role in the propagation over the WNP, whereas the mean vertical wind shear mechanism is the major driver over the IO. Lowering TP significantly reduces sea surface temperature (SST) anomalies to the north of BSISO center due to the enhanced surface wind and latent heat flux anomalies. This air-sea interaction reduces upward transport of heat and moisture from surface to lower troposphere, weakening the northward propagation over the WNP. This study implies changes in SST patterns under global warming may influence BSISO propagation.

Plain Language Summary A heavy rainfall system propagates slowly from the equatorial western Pacific to the south China Sea and north of the Philippine Sea on a 20–70-day time scale. This rainfall system affects the onset of East Asia monsoon and extreme weather including typhoons. Therefore, a better understanding of the dominant processes of the northward propagation of this heavy rainfall system may contribute to reducing its social and economic damage. For this purpose, we performed a set of climate model experiments. We found that lowering the Tibetan Plateau significantly decreases the meridional gradient of the warm SST anomalies associated with the heavy rainfall system, suggesting that the air-sea interaction plays a dominant role in the BSISO northward propagation over the Western North Pacific. In contrast, vertical shear of zonal winds and associated positive vorticity anomalies, the major driver over the Indian Ocean, does not contribute to the northward movement over the Western North Pacific.

Key Points:
- Northward propagation of BSISO over the WNP and IO is significantly weakened if the elevation of the Tibetan Plateau is lowered
- The air-sea interaction is the major driver for BSISO propagation in the WNP but the vertical wind shear mechanism is the key in the IO
- Lowering the TP enhances surface wind and latent heat flux, weakening meridional SST gradient and BSISO northward propagation over the WNP

Supporting Information:
- Supporting Information S1

Correspondence to:
J.-Y. Lee,
juneyi@pusan.ac.kr

Citation:
Yang, Y.-M., Lee, J.-Y., & Wang, B. (2020). Dominant process for northward propagation of boreal summer Intraseasonal oscillation over the Western North Pacific. *Geophysical Research Letters*, *47*, e2020GL089808. https://doi.org/10.1029/2020GL089808

Received 15 JUL 2020
Accepted 3 NOV 2020
Accepted article online 9 NOV 2020

1. Introduction

Boreal summer intraseasonal oscillation (BSISO) exhibits robust northward propagation in the Western North Pacific (WNP) as well as in the Indian Ocean (IO) during the Northern Hemisphere (NH) summer (e.g., Hsu & Weng, 2001; Wang & Rui, 1990; Zhu & Wang, 1993). In the WNP and East Asia sector, the BSISO northward propagation begins near the equator, extends to subtropical western Pacific, affecting the East Asian summer monsoon (e.g., Hsu et al., 2017; Lee et al., 2013, 2017; Li et al., 2015; Wang & Xie, 1997; Yang et al., 2010), typhoon activities (Goswami et al., 2003; Kikuchi et al., 2009; Maloney & Hartmann, 2001; Moon et al., 2018), and extreme weather events (Hsu et al., 2016, 2017; Moon et al., 2013).

Many processes and mechanisms have been suggested to explain the northward propagation of BSISO in the WNP and the IO, including air-sea interaction, vorticity anomalies induced by vertical wind shear, and meridional moisture advection. Hsu and Weng (2001) found that positive feedback between the anomalous circulation and convection leads to enhanced evaporation over the oceans (e.g., South China Sea) and moisture transport northeastward. Kemball-Cook and Weare (2001) suggested that sea surface temperature (SST) is likely to be warmer north of the BSISO precipitation center due to enhanced net surface flux by reduced

wind speed and latent heat flux, which is more favorable for convection moving northward. The increased SST anomalies induced by air-sea interaction enhance convective instability to the north of convection, thus moving the convection northward (Fu et al., 2003; Fu & Wang, 2004; Zheng et al., 2004). Katsumata et al. (2011) proposed that premoistening due to warmer SST anomalies north of ISO center might be critical for northward propagation of ISO precipitation.

The dynamic theories encompassing wave dynamics and vorticity-wind shear interaction have been proposed to explain northward propagation of BSISO (Drbohlav & Wang, 2005; Jiang et al., 2004; Wang & Xie, 1997). Jiang et al. (2004) suggested that the northward propagation of ISO convection may be generated by the boundary layer (BL) moisture convergence to the north of the BSISO precipitation center. The BL moisture convergence is caused by the barotropic vorticity anomalies that are converted from the baroclinic vorticity in the presence of the mean state vertical shear (Wang & Xie, 1996). Using a climate model, DeMott et al. (2013) found that the boundary layer moisture advection and barotropic vorticity effect together contribute to northward propagation of BSISO precipitation. Yang, Wang, and Lee (2019) demonstrated that the interaction among wave dynamics, vorticity anomalies, and vertical wind shear is the dominant process for BSISO northward propagation in the IO.

On the other hand, a few studies focused on the role of convective momentum transport, which may induce boundary layer convergence by a secondary meridional circulation under the presence of an easterly shear (Kang et al., 2010; Liu et al., 2015). Additionally, the effect of shallow convection has been emphasized by Liu et al. (2018) and Abhik et al. (2013). They suggested that the shallow convection may help BSISO propagate northward by generating shallow convection at the north of the BSISO convective center. Stephens et al. (2002) and Simmons et al. (2007) used satellite data and found that cloud water in the lower troposphere occurs north of the ISO convection center, which may contribute to the northward propagation of BSISO.

Many climate or Earth system models have been involved to improve BSISO simulation. Our study utilizes a recently developed Earth system model, the Nanjing University of Information Science and Technology (NUIST) Earth System Model version 3 (NESM3) (Cao et al., 2018; Yang, An, et al., 2020). The NESM3.0 reproduces reasonable climatology and realistic MJO and BSISO (Yang, Lee, & Wang, 2019; Yang, An, et al., 2020; Yang, Wang, et al., 2020; Yang & Wang, 2019). In the model simulations, the northward propagation of BSISO is well reproduced over both the WNP and IO.

Our previous study demonstrates that the vorticity advection under the mean vertical wind shear is the major driver for BSISO propagation in the IO (Yang, Wang, & Lee, 2019). However, over the WNP, the vertical wind shear is significantly weaker than that over the IO. This study aims to test whether such a mechanism still works in the WNP through coupled climate model experiments. In a broader perspective, we examine the roles of air-sea interaction, meridional moisture advection, and vorticity anomalies by zonal vertical shear on BSISO northward propagation. We change the mean states of circulation and temperature by lowering the Tibetan Plateau (TP) orography and adding a new shallow convective scheme.

The method and model experiments are described in section 2. We examine dominant mechanisms for BSISO northward propagation in different mean states and parameterization using various diagnostics in section 3. The profound mechanisms responsible for BSISO northward propagation are discussed in section 4. Section 5 summarizes our findings.

2. The Model and Diagnostic Methods

2.1. Model and Experiments

The NESM3.0 includes atmosphere, ocean, land, and sea-ice components. The details of the model are described in Cao et al. (2018) and Yang, An, et al., (2020). The horizontal resolution of the atmosphere model is T63 (about 200 km) and its vertical resolution is 47 levels. The ocean model has 46 layers vertically. The horizontal resolution of the ocean model varies meridionally: it has a fine resolution (about 1/3°) over the equatorial region and becomes coarse resolution (1°) in polar regions. The sea ice model has four layers with a horizontal resolution of about 1°.

To obtain the effect of different mean state on BSISO northward propagation, we conduct three experiments: (1) the NESM3.0 with observed orography (TP100); (2) orography reduced by 50% (TP50); and (3) flat orography (TP00) over the TP region (60–110°E, 25–45°N). Figure 1 of Yang, Wang, and Lee (2019) shows a

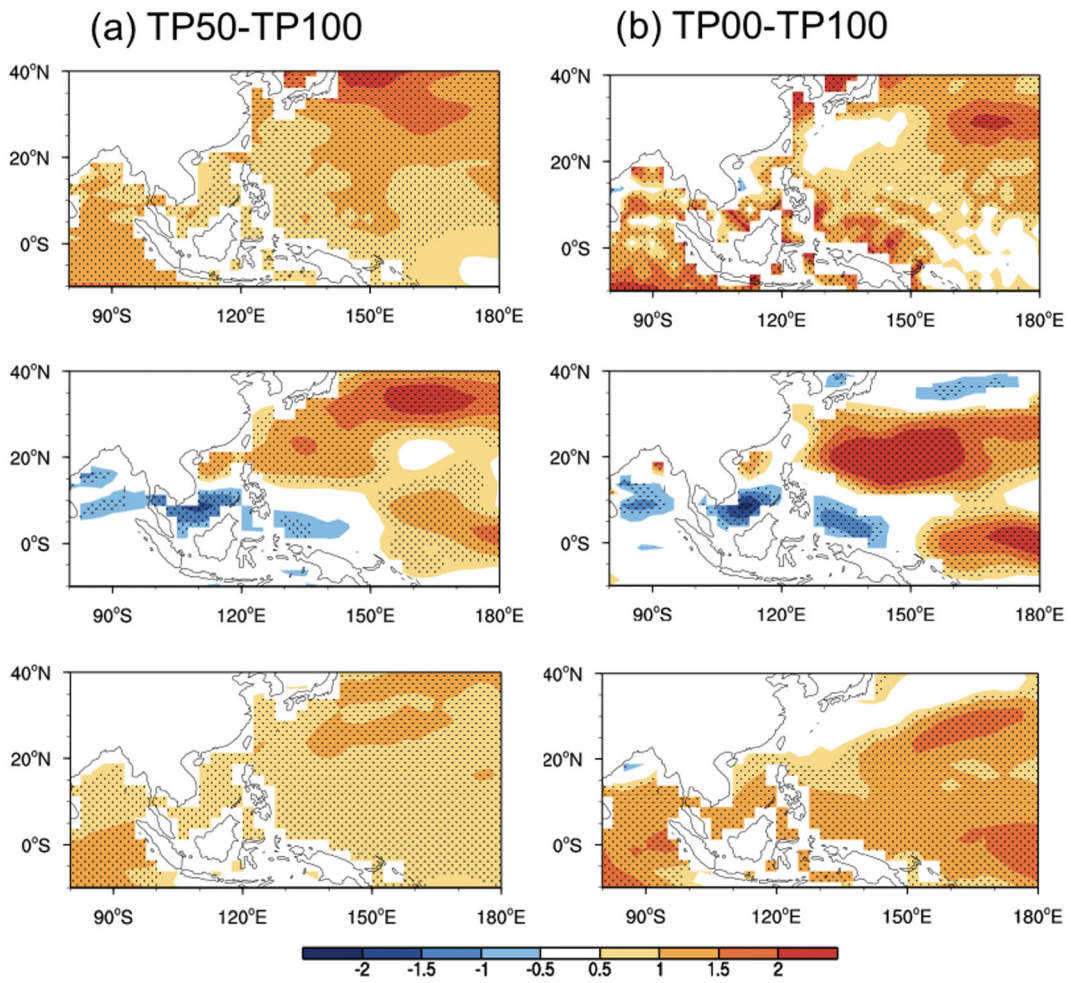

Figure 1. Differences in June–August mean-state sea surface temperature (K) (upper panel) and 850-hPa zonal wind (m s^{-1}) (middle panel), and lower-tropospheric moisture at 850 hPa (g kg^{-1}) (lower panel) between (a) TP50 and TP100 and (b) TP00 and TP100. Stippling indicates the region with statistically significant change at a 95% confidence level based on *t* test.

horizontal map of orography over the TP region used in the experiments. We smooth the boundaries of the orographic area based on the method of Cannon et al. (2017) to remove undesired numerical noises. Also, we reduce all external parameters associated with the orography effects (e.g., orographic standard deviation, slope, anisotropy, angle, peak elevation, valley elevation, and mean orography data) accordingly. We set up the same model configuration and parameter values for all three experiments except the orography. There are two reasons for generating different mean state by lowering the elevation of the TP instead of nudging to an idealized wind or SST field directly. First, we may obtain an energy-balanced mean state in the current approach. When we use wind field nudging methods, the SST conditions are not well-matched with the modified wind field because the wind-driven SST change is not fully considered in the model. Second, we would like to see the impact of the elevation of the Tibet Plateau on ISO propagation itself. Previous studies (e.g., Lee et al., 2015; Wang & Xie, 1997) revealed that lowering the Tibetan Plateau changes seasonal-mean state and Asia monsoon. Therefore, we expect that lowering the Plateau can affect ISO simulation significantly.

Previous results have emphasized the importance of shallow convective heating and moistening in the BL and lower troposphere for BSISO propagation. In the context of these findings, we have modified the shallow convection in the model. In the model simulation with the original convective scheme, the vertical mixing between the lower troposphere and the top of BL is insufficient, thus shallow convection mainly occurs in

the BL (900–1000 hPa) and/or in the lower troposphere (600–700 hPa). To fix this problem, a bottom-heavy diffusivity in the shallow convection scheme (SHC) was added to the model (Yang & Wang, 2019), which is modified from the scheme of Tiedtke et al. (1988). This scheme is described by the following diffusive terms for grid mean dry static energy s and specific humidity q (Tiedtke et al., 1988)

$$\frac{\partial \overline{s}}{\partial t} = \frac{1}{\overline{\rho}} \frac{\partial}{\partial z} \left\{ \overline{\rho} K \frac{\partial}{\partial z} \left(\overline{s} - L\overline{l} \right) \right\} \tag{1}$$

$$\frac{\partial \overline{q}}{\partial t} = \frac{1}{\overline{\rho}} \frac{\partial}{\partial z} \left\{ \overline{\rho} K \frac{\partial}{\partial z} \left(\overline{q} + \overline{l} \right) \right\} \tag{2}$$

where l denotes cloud liquid water content, ρ is the air density, L the latent heat, t the time, and z the height. The coefficient K is the eddy diffusivity, which is a prescribed function of height or pressure. Our shallow convection scheme implements a specific vertical profile of vertical mixing below 600 hPa. The vertical mixing near 925 hPa is heavy and then gradually reduces to zero at 600 hPa. When we implemented this shallow convection to the earlier NESM3.0, it effectively enhanced shallow convection between the BL and the lower troposphere. It has been suggested that the lower tropospheric heating by shallow convection may play a role in improving BSISO simulation (Abhik et al., 2013; Liu et al., 2018). The shallow convective scheme used in this study has the potential to produce better BSISO simulation if lower tropospheric heating is enhanced.

We carry out 50-year integrations for all experiments with fixed external forcings (1990s). and analyze the last 15-year simulation data of total simulation. We adopt initial conditions from a historical run based on the CMIP6 protocols.

2.2. The Data and Diagnostic Methods

As a reference, the Global Precipitation Climatology Project (GPCP) daily data (Adler et al., 2003) are used for precipitation and the European Center for Medium-Range Weather Forecast Reanalysis (ERA) Interim daily data (Dee et al., 2011) for circulation during 1997–2014. We adopt a 20–70-day band-pass filter to obtain the ISO signal during the boreal summer season (1 May to 31 October). We analyze the relationship between circulation, SST and moisture, and ISO northward propagation based on dynamics-based diagnostics. The vertical shear is defined by the difference in zonal winds between 200 and 850 hPa (U200–U850) averaged over 125°E and 145°E.

3. Effects of Lowering TP Orography on Mean Fields and BSISO

3.1. Changes in the Boreal Summer Mean Climate

Figure 1 shows mean-state differences in SST, horizontal winds, and lower specific humidity at 850 hPa between the TP100 and TP50 and between the TP100 and TP00 during boreal summer (June–August). Compared to the TP100, the TP50 shows moderate warming from the equator to 20°N. In the TP00, stronger warming occurs in the Philippine Sea but weak warming in the East China Sea compared to those of the TP100, suggesting that the meridional gradient of the mean SST is reduced from 0° to 30°N. The weakened meridional gradients of mean SST can be less favorable for the BSISO northward propagation. The TP50 simulates easterly anomalies over western subtropical Pacific (5°S to 15°N) and westerly anomalies over 20–40° N. The easterly anomalies may weaken BSISO northward propagation by reducing the vertical shear. In the TP00, the anomalous easterlies are increased, suggesting that TP00 may yield even more weakened vertical shear. The TP50 produces relatively humid air in the WNP and there is no significant change in the meridional gradient of mean-state moisture. The TP00 shows a reduced meridional gradient change of mean-state moisture between 0 and 25°N, which is expected to be less favorable for the northward propagation of BSISO.

In sum, the lowering TP orography leads to decreased meridional gradients of the SST and moisture in the western subtropical Pacific (and East Asia) and enhanced anomalous surface easterly in the WNP. Those mean state changes, in theory, are expected to be unfavorable for the northward propagation of BSISO in the WNP and East Asian summer monsoon region.

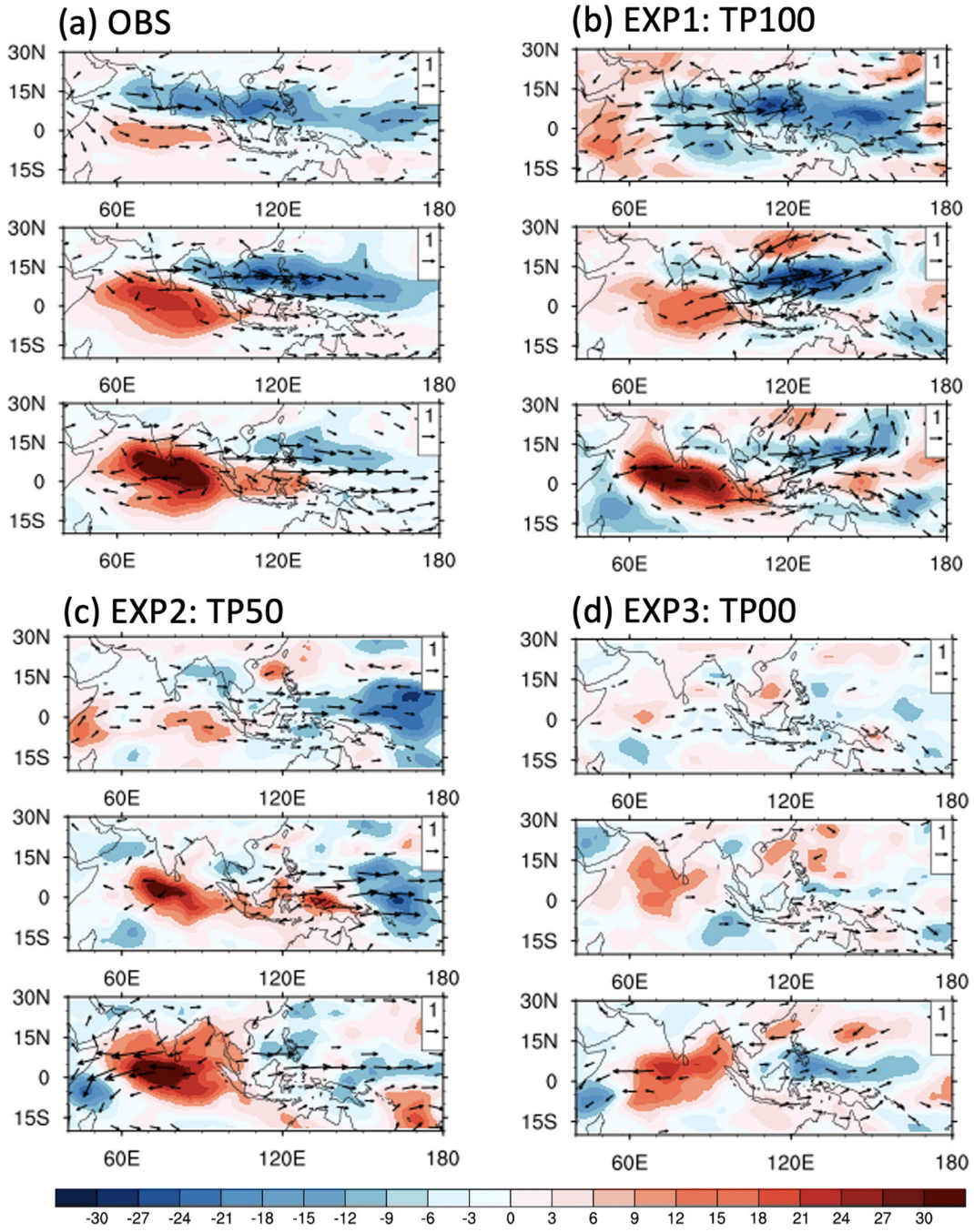

Figure 2. The life cycle composite of OLR (shading) and 850-hPa wind (vector) anomaly reconstructed based on PC1 and PC2 of BSISO1 in Phases 4 (upper), 5 (middle), and 6 (bottom) obtained from (a) observation, (b) TP100, (c) TP50, and (d) TP00. The composite life cycles have a moderate amplitude (1.0). We defined eight phases of ISO based on Lee et al. (2013), the wind vectors are represented with statistical significance at a 95% confidence level based on *t* test.

3.1.1. Changes in BSISO Properties

Analysis of climate model experiments indicates that the mean-field changes due to lowering the TP orography indeed systematically weaken the BSISO northward propagation over the WNP, providing a good opportunity to examine major mechanisms driving the propagation. However, the response of BSISO variance to the mean state changes is not linear in the TP50 and TP00 (Figure S1). Compared to the TP100, the BSISO variance is strengthened in the South China Sea and subtropical WNP over 15°N but weakened in the

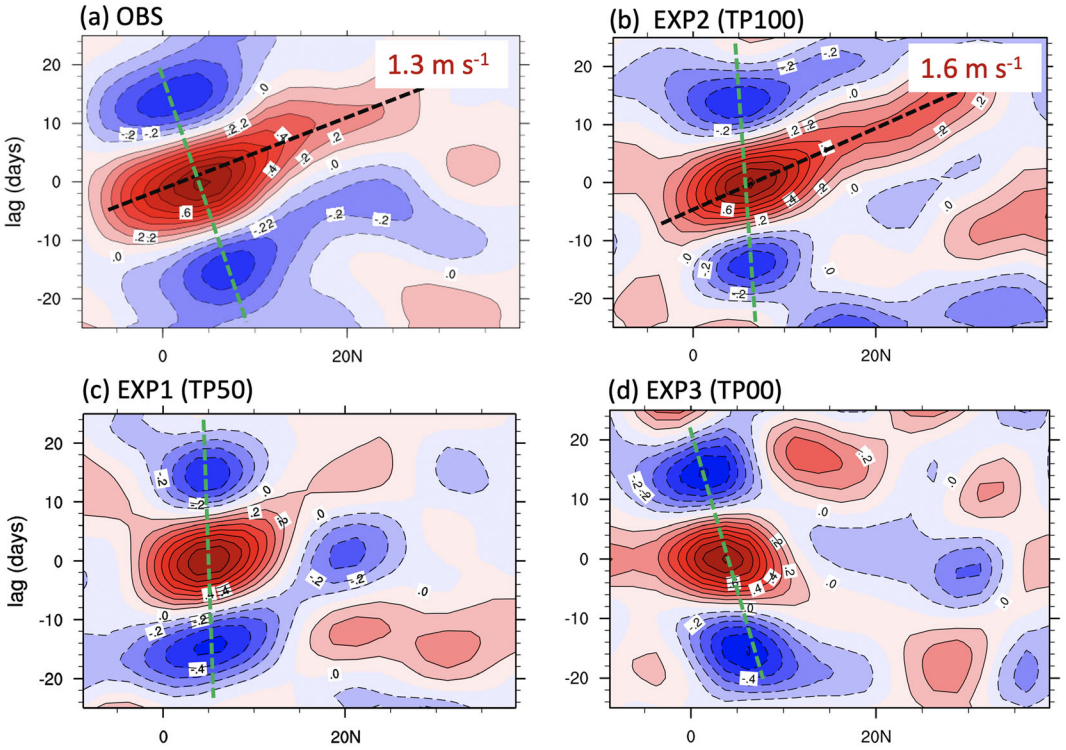

Figure 3. Propagation of ISO precipitation as depicted by the lead-lag correlation of 20–70 day filtered precipitation averaged over 125–145°E from (a) observation and model simulations with (b) observed topography, (c) 50% of observed topography, and (d) no topography over the Tibetan plateau region during boreal summer (May–October). The ISO precipitation averaged over 125–145°E and 0°S to 5°N was used as a reference for calculating the correlation. The black dashed line shows the northward propagation of the BSISO and the red number represents the speed of propagation. The green dashed line shows the movement of the maximum convective activity center.

Philippine Sea and subtropical WNP below 15°N in the TP50. However, the TP00 exhibits a significant reduction of BSISO variance over most of WNP compared to the TP100 and TP50.

To examine the characteristics of BSISO propagation over the WNP in the models, the Phases 4 to 6 in the composite life cycles of outgoing longwave radiation (OLR) and horizontal winds at 850 hPa associated with the BSISO are shown in Figure 2. These phases are determined by the first two major modes of BSISO during May–October. We first calculated daily anomalies of OLR and zonal wind at 850 hPa (U850) (10°S to 10°N, 40–160°E) and applied multivariate empirical orthogonal function analysis (Lee et al., 2013). Eight phases are defined based on the first and second EOF mode, representing the canonical northward propagating mode (BSISO1). The observation shows strong BSISO convective anomalies in the Maritime continent at Phase 4 (the top panel of Figure 2a), and they move eastward and northward. The BSISO anomalies are intensified and reach the WNP at Phase 5 (the middle panel of Figure 2a). The strong convection anomaly moves northward from the southern Philippine Sea to the South China Sea and extends eastward to the western Pacific at Phase 6 (the lower panel of Figure 2a). The BSISO convective anomalies weaken and decay at Phases 7 and 8 (not shown). The TP100 successfully captures the observed northward propagation of BSISO in the WNP. The simulated BSISO is more intense than the observed counterpart south of the Philippine Sea (Figure 2b). The convection anomalies move northward from south of the Philippine Sea to the subtropical western Pacific. In the TP50, the ISO convection in the west of the Philippine occurs at Phase 4 and it seems to move both northward to the subtropical western Pacific and southward to the equator at Phase 5. The propagation of ISO convection is weakened in Phase 6 (Figure 2c). However, the BSISO structure in the TP50 is not well organized compared to that of observation and TP100. The TP00 simulation shows very weak ISO anomalies at Phase 4. The convective anomalies weaken and disappear at Phase 5, suggesting that the TP00 fails to simulate northward propagation in the western Pacific (Figure 2d). Note that the failure of TP00 for the northward propagation of the ISO is attributable to not only the missing

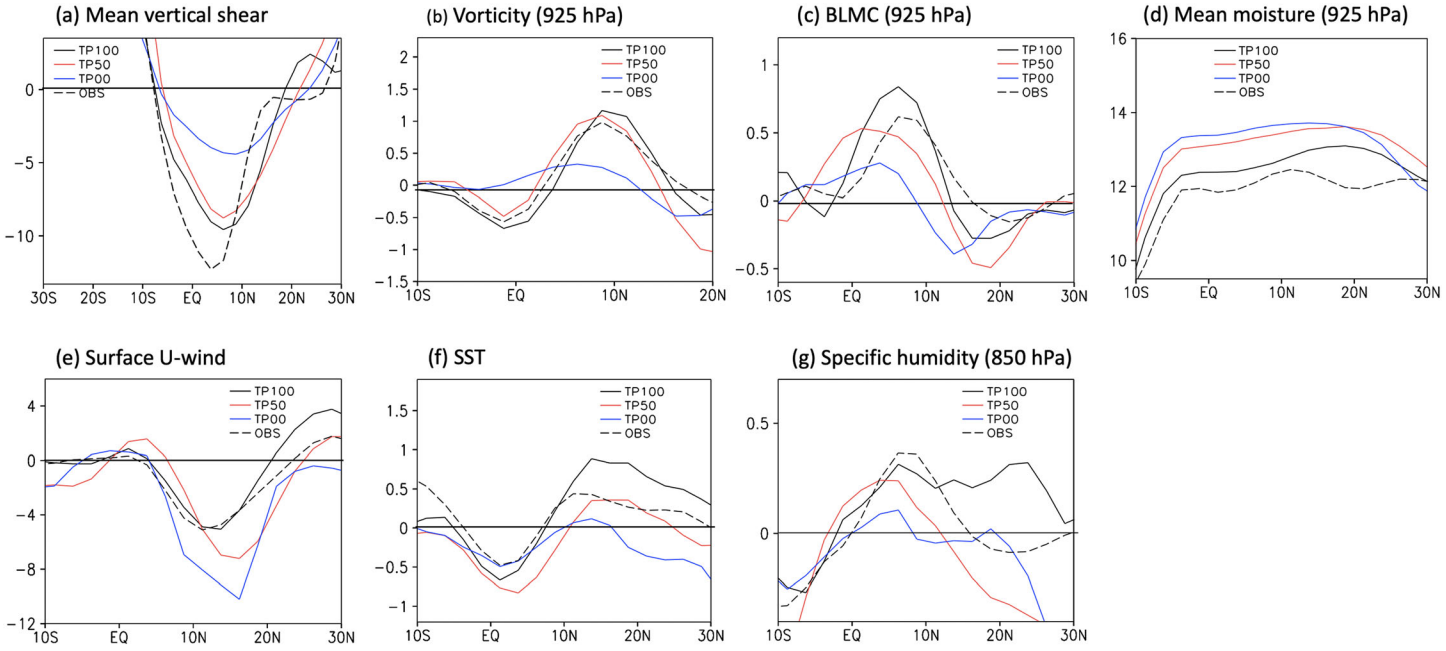

Figure 4. Meridional structure of May–November (a) mean-state zonal shear (U_{200}–U_{850}) and (d) mean specific humidity (925 hPa) averaged over 125–145°E from observation (dashed black) and models. Meridional variation of the regressed ISO (b) relative vorticity (s^{-1}) at 925 hPa, (c) BL moisture convergence (day^{-1}) at 925 hPa, (e) surface wind (m s^{-1}), (f) SST (k) and (g) specific humidity (850 hPa) averaged over 125–145°E from observation (dashed black) and model simulations. The 20–70 day filtered precipitation anomaly averaged over 5°S to 5°N and 125–145°E was used as a reference for calculating regression.

processes driving the northward propagation (e.g., incorrect vorticity by the reduced vertical shear and/or air-sea interaction) but also the weak initial intensity.

Figure 3 shows the meridional lead–lag correlation of BSISO precipitation in the WNP. Because strong BSISO northward propagation starts from south of the Philippine Sea, the BSISO precipitation center at the equatorial western Pacific (125–145°E, 0°S to 5°N) was used as a reference. Observations show that the BSISO precipitation moves northward with a phase speed of about 1.3 m s^{-1} from south of the Philippine Sea to the subtropical western Pacific. The TP100 (Figure 3b) successfully reproduces the ISO northward propagation with a larger magnitude and faster phase speed of about 1.6 m s^{-1}. In the TP50, the signal for northward propagation of ISO weakens when compared to TP100 (Figure 3c). The TP00 simulates very weak northward propagation (Figure 3d). The BSISO convection seems to be standing in the WNP or moves southward. These results suggest that the lowering orography tends to worsen the northward propagation of the ISO simulation significantly. Note that observation shows a southward tilt with the time of the maximum activity, suggesting a southward group velocity. TP100 fails to simulate the tilt but the TP00 experiment captures a similar feature, suggesting that the change of mean state also affect group velocity simulation of BSISO. A cautious note is that the propagation of local convection extrema does not necessarily indicate the propagation of the wave envelopes or the group velocity (Chen & Wang, 2018).

4. Causes of the Changes of ISO Simulations With Reduced Orography

By analyzing the circulation and thermodynamic fields as well as the lower tropospheric moisture and SST, we examine how the mean state change affects the BSISO propagation over the WNP. The lowering orography over the TP region changes the boreal summer mean vertical shear of the zonal wind by modifying circulation and temperature fields (Figure 4a). The observation shows a significant easterly vertical shear from south of Philippine Sear to subtropical western Pacific (8°S to 12°N) and the vertical shear reaches a peak value around 5°N. The TP100 reproduces easterly vertical shear well compared to observations but the maximum vertical shear is relatively weak (80%). The vertical shear from the TP50 is slightly weaker than that of the TP100. The TP00 simulates very weak vertical shear from south of the Philippine Sea to subtropical

western Pacific. When we compare the TP100 with TP00, vertical shear is reduced due to the anomalous easterlies in the lower troposphere, which results from the reduced TP dynamic and thermodynamic effects.

The change of vertical zonal wind shear can generate a barotropic vorticity anomaly by the coupling of the baroclinic and barotropic modes by mean vertical shear (Wang & Xie, 1997; Xie & Wang, 1996). Yang, Wang, and Lee (2019) demonstrated that the vorticity anomaly under the mean vertical wind shear is the major driver for the BSISO northward propagation over the IO. The lower tropospheric vorticity anomalies regressed on the 20–70 day filtered precipitation averaged over the western Pacific (0–5°N, 125–145°E) are shown in Figure 4b. In observation, positive vorticity anomalies are seen from 5°N to 15°N, and its peak is located around 10°N, which is consistent with the range of northward propagation of the ISO precipitation center (e.g., Jiang et al., 2004). The TP100 experiment captures the observed vorticity anomalies but its magnitude is larger than the observed. The magnitude of the vorticity in TP50 is almost the same as that of TP100, which may be attributed to its comparable vertical shear. In the TP00, the magnitude of vorticity anomalies is very weak from 10°S to 15°N, which may be due to the very weak vertical shear. These model experiments suggest that the vorticity anomaly changes with the magnitude of vertical wind shear. However, the magnitude of cyclonic vorticity in the TP50 is similar with observation but the northward propagation signal of ISO convection from the TP50 is relatively weak, implying that the vorticity anomalies may not be the primary factor for the generation of the next convection center north of the ISO center in the WNP.

The BL moisture convergence (BLMC) may be generated by changes in vorticity anomalies (Figure 4c). It is observed that the BLMC is almost zero at the BSISO center and has a peak around 10°N with a northward weakening. This indicates that the next convection center may be generated to the north of the current ISO center. The TP100 reproduces the observed BLMC well but the TP50 simulates weaker BLMC than that of the TP 100, although they produce similar vorticity anomalies. Comparisons between Figures 4b and 4c indicate that the vorticity anomalies may play a minor role in generating BLMC in the western Pacific, and other mechanisms such as moisture-convection feedback and air-sea interaction may contribute to the generation of the BLMC to the north of the BSISO center. The TP00 has a peak near the equator and becomes negative around 5°N, suggesting that TP00 does not simulate the BLMC to the north of the ISO convection center, which is consistent with its failure to simulate the ISO northward propagation.

We examine other mechanisms that may be critical for BSISO northward propagation. First, BL moisture advection by the winds associated with BSISO was tested (DeMott et al., 2013; Jiang et al., 2004). The convection may occur at the north of the BSISO center by increased specific humidity. Figure 4d shows the meridional structure of mean specific humidity. The observation shows a low specific humidity near the equator and it increases northward, reaching a peak near 12°N, suggesting that it favors convection occurring to the north of the ISO center. The TP100 reproduces the observed pattern of specific humidity over 10°S to 20°N but the magnitude is relatively strong, which may be due to the warmer SST there. In the TP50, the moisture content is higher than observation over 5°S to 25°N, but the meridional gradient of moisture is smaller than that of the TP100, which is consistent with the weak northward propagation of BSISO over the WNP (e.g., Figure 3c). The TP00 shows flatter meridional gradients of moisture over 0–25°N, suggesting that moisture condition in the TP00 may be unfavorable for northward propagation of the BSISO center. Indeed, the TP00 fails to capture BSISO northward propagation (e.g., Figure 3c). These model results suggest that the proper meridional structure of BL moisture may contribute to the subsequent ISO northward propagation.

We also test whether the air-sea interaction mechanism contributes to ISO northward propagation. Figure 4f shows the meridional structure of the SST anomalies regressed on the equatorial BSISO convection (125–145°E, 0–5°N). It is observed that cold SST anomalies occur near the BSISO precipitation center due to weakened downward solar radiation by strong ISO convection, and the warm SST anomalies are seen over (8–30°N), favoring for the next convection occurring north of the ISO center. In the TP100, the meridional pattern of warm SST anomalies over 5–30°N is similar to the observation but its magnitude is larger than the observation. The TP50 also simulates warm SST anomalies to the north of equatorial ISO with relatively weak magnitude. However, the TP00 simulates cold SST anomalies over 0–30°N. Compared with the northward propagation of BSISO precipitation shown in Figures 3, the signals of the BSISO northward propagation deteriorate with reducing the meridional gradient of SST anomalies by lowering TP elevation. This indicates that the interaction between atmosphere and ocean may be an important mechanism in supporting ISO northward propagation in this experiment. Correspondingly, the moisture anomalies tend to

increase to the north of the BSISO convection center (Figure 4g), which may be associated with warmer SST anomalies. Note that the change in SST associated with BSISO may result from a change in the latent heat flux by enhancing surface wind anomalies. Figure 4e shows regressed surface zonal wind anomalies on BSISO precipitation. The TP100 simulates observation reasonably well. The easterly anomalies over WNP tend to increase with lowering TP elevation. This suggests that surface wind and associated latent heat flux increase at the north of the ISO convection center, inducing the cooling there.

The mechanisms for BSISO northward propagation may be dependent on the model parameterizations. To check whether air-sea interaction as a dominant mechanism or process working in other models, we also conduct a model experiment using NESM with the modified shallow convection (hereafter "SHC"). Figure S2a shows the meridional lead-lag correlation diagrams of ISO precipitation in the western Pacific from the SHC. The ISO northward propagation occurs over 5–20°N with a larger magnitude than observation. Figure S2b shows that the magnitude of zonal vertical shear is not closer to the observation but the SHC simulates warmer SST anomalies than the TP50 over 5–20°N, suggesting that the air-sea interaction may be critical for BSISO northward propagation. On the other hand, the TP50 simulates a relatively weaker northward propagation of BSISO than the SHC, which is attributable to the colder SST anomalies than that of the SHC. It suggests that the air-sea interaction may be important for BSISO northward propagation in both models.

5. Conclusion and Discussion

We explore dominant processes for BSISO northward propagation in the WNP including the vertical zonal wind shear-relative vorticity mechanism, the role of meridional gradients of the mean specific humidity, and the air-sea interaction process by examining the NESM3.0 numerical simulations. The NESMv3.0 model reproduces the observed pattern of the ISO northward systematically from south of the Philippine Sea to the subtropical western Pacific.

Analysis of the northward propagating BSISO structure from climate model experiments shows that air-sea interaction plays a major role in the northward propagation of BSISO precipitation over the WNP. The lowering TP elevation reduces warm SST anomalies associated with BSISO center at the north of ISO center, suggesting that the ensuing convection may be prohibited over there, and thus northward propagation is weakened. Other proposed mechanisms that attempt to explain the northward propagation of ISO are also tested. We examined the mechanisms of the meridional moisture advection of the mean specific humidity and the vorticity anomalies generated by zonal vertical shear. The meridional gradients of the mean moisture are reduced by lowering the TP elevation, which is consistent with the weakened northward propagation of ISO convection. Also, the TP50 experiment shows similar positive vorticity anomalies by enhanced zonal vertical shear as in the TP100 but corresponding northward propagations are significantly weakened. This suggests that positive vorticity anomaly generated by zonal vertical shear is not a major factor for northward propagation of the BSISO in the western Pacific. On the other hand, the SHC experiment shows better northward propagation of the ISO precipitation than the TP50. The SST anomalies north of the BSISO center from SHC are much warmer than that of TP50, but the magnitude of zonal vertical shear is similar to that of TP50. This indicates air-sea interaction is a key factor for the ISO northward propagation and the zonal vertical shear mechanism is not essential for simulating northward propagation in the WMP region in this model.

Previous studies focusing on northward propagation of BSISO convection in the eastern IO have suggested that vorticity anomalies by zonal vertical shear may be the dominant factor for northward propagation of ISO (DeMott et al., 2013; Yang, Wang, & Lee, 2019). We speculate that because much warmer SST and more abundant moisture occur in the WNP compared to those in the eastern IO, convection may be mainly generated due to upward transport of moisture by surface fluxes processes rather than dynamical processes in the WNP. This may be one of the reasons for the more profound influence of air-sea interaction processes in the WNP.

One of limitations in this study is to use a single model for the numerical experiments to test our hypotheses. Further studies based on different climate models may be useful to examine the degree of model-dependence of the results. Generally speaking, the ISO simulation is sensitive to convective parameterizations (including shallow convective scheme) as well as other physical processes and the conclusion derived here warrants further confirmation or modification. For example, we examined the impact of the

"convective trigger" on the northward propagation of BSISO. We added a boundary depth-dependent convective trigger to the convective scheme (hereafter "TRIG"; Yang et al., 2018; Yang & Wang, 2019). This trigger is based on the Tokioka constraint (1988). The latitude-time structures in the western Pacific from the model with and without the convective trigger were shown in Figure S3. The TRIG successfully reproduces ISO northward propagation with reasonable magnitude and phase speed of about 1.2 m s^{-1}. These results suggest that the modified parameterizations tend to improve the northward propagation of the ISO simulation significantly.

Our results suggest that the changes in SST patterns under global warming may influence BSISO propagation. We further conducted a global warming experiment (TP100_SSP245) using NESM3.0 under the Shared Socioeconomic Pathway 2–4.5 (SSP245) scenario in coupled model intercomparison Phase 6 (CMIP6). Compared to TP100 with 1990′ fixed forcing, TP100_SSP245 shows a slower propagation speed (1.2 m s^{-1}), which is about 60–70% of that of the TP100 (1.6 m s^{-1}) (Figure S4). The reduction of the speed may be attributed to the reduced meridional gradient of the SST in the western Pacific in response to global warming. We also expect that global warming may change BSISO variance including the maximum magnitude of precipitation variability. A detailed analysis of the possible mechanisms will be investigated in a future study.

Data Availability Statement

The data are available at https://figshare.com/articles/dataset/daymon2_nc/12651554.

Acknowledgments

This work is funded by the National Key Research and Development Program of China (Grant No. 2016YFA0600401) and the National Natural Science Foundation of China (Grant No. 41420104002) as well as the National Science Foundation (Climate Dynamics Division) Award No. AGS-1540783. This is the Earth System Modeling Center (ESMC) publication no. XXX. J.-Y. Lee acknowledges the support from the Institute for Basic Science (project code IBS-R028-D1) and the National Research Foundation (NRF-2019R1I1A3A0105829) in Korea.

References

Abhik, S., Halder, M., Mukhopadhyay, P., Jiang, X., & Goswami, B. (2013). A possible new mechanism for northward propagation of boreal summer intraseasonal oscillations based on TRMM and MERRA reanalysis. *Climate Dynamics*, *40*, 1611–1624. https://doi.org/10.1007/s00382-012-1425-x

Adler, R. F., Huffman, G. J., Chang, A., Ferraro, R., Xie, P. P., Janowiak, J., et al. (2003). The version-2 global precipitation climatology project (GPCP) monthly precipitation analysis (1979–present). *Journal of Hydrometeorology*, *4*(6), 1147–1167. https://doi.org/10.1175/1525-7541(2003)004<1147:TVGPCP>2.0.CO;2

Cannon, F., Carvalho, L. M. V., Jones, C., Norris, J., Bookhagen, B., & Kiladis, G. N. (2017). Effects of topographic smoothing on the simulation of winter precipitation in High Mountain Asia. *Journal of Geophysical Research: Atmospheres*, *122*, 1456–1474. https://doi.org/10.1002/2016jd026038

Cao, J., Wang, B., Yang, Y.-M., Ma, L., Li, J., Sun, B., et al. (2018). The NUIST Earth system model (NESM) version 3: Description and preliminary evaluation. *Geoscience Model Development*, *11*, 2975–2993. https://doi.org/10.5194/gmd-11-2975-2018

Chen, G., & Wang, B. (2018). Does the MJO have a westward group velocity? *Journal of Climate*, *31*(6), 2435–2443. https://doi.org/10.1175/JCLI-D-17-0446.1

Dee, D. P., Uppala, S. M., Simmons, A. J., Berrisford, P., Poli, P., Kobayashi, S., et al. (2011). The ERA-interim reanalysis: Configuration and performance of the data assimilation system. *Quarterly Journal of the Royal Meteorological Society*, *137*(656), 553–597. https://doi.org/10.1002/qj.828

DeMott, C. A., Stan, C., & Randall, D. A. (2013). Northward propagation mechanisms of the boreal summer intraseasonal oscillation in the ERA-interim and SP-CCSM. *Journal of Climate*, *26*, 1973–1992. https://doi.org/10.1175/JCLI-D-12-00191.1

Drbohlav, H.-K. L., & Wang, B. (2005). Mechanism of the northward propagating intraseasonal oscillation: Insights from a zonally symmetric model. *Journal of Climate*, *18*, 952–972. https://doi.org/10.1175/JCLI3306.1

Fu, X., & Wang, B. (2004). Differences of boreal summer intraseasonal oscillations simulated in an atmosphere-ocean coupled model and an atmosphere-only model. *Journal of Climate*, *17*, 1263–1271. https://doi.org/10.1175/1520-0442(2004)017<1263:DOBSIO>2.0.CO;2

Fu, X., Wang, B., Li, T., & McCreary, J. P. (2003). Coupling between northward-propagating, intraseasonal oscillations and sea surface temperature in the Indian Ocean. *Journal of the Atmospheric Sciences*, *60*, 1733–1753. https://doi.org/10.1175/1520-0469(2003)060<1733:CBNIOA>2.0.CO;2

Goswami, B. N., Ajayamohan, R. S., Xavier, P. K., & Sengupta, D. (2003). Clustering of synoptic activity by Indian summer monsoon intraseasonal oscillations. *Geophysical Research Letters*, *30*(8), 1431. https://doi.org/10.1029/2002GL016734

Hsu, H.-H., & Weng, C.-H. (2001). Northwestward propagation of the intraseasonal oscillation in the Western North Pacific during the boreal summer: Structure and mechanism. *Journal of Climate*, *14*, 3834–3850. https://doi.org/10.1175/1520-0442(2001)014<3834:NPOTIO>2.0.CO;2

Hsu, P.-C., Lee, J.-Y., & Ha, K.-J. (2016). Influence of boreal summer intraseasonal oscillation on rainfall extremes in southern China. *International Journal of Climatology*, *36*, 1403–1412. https://doi.org/10.1002/joc.4433

Hsu, P.-C., Lee, J.-Y., Ha, K.-J., & Tsou, C.-H. (2017). Boreal summer intraseasonal oscillation on heat waves in monsoon Asia. *Journal of Climate*, *30*, 7191–7211. https://doi.org/10.1175/JCLI-D-16-0505.1

Jiang, X., Li, T., & Wang, B. (2004). Structures and mechanisms of the northward propagating boreal summer intraseasonal oscillation. *Journal of Climate*, *17*, 1022–1039. https://doi.org/10.1175/1520-0442(2004)017<1022:SAMOTN>2.0.CO;2

Kang, I.-S., Kim, D., & Kug, J.-S. (2010). Mechanism for northward propagation of boreal summer intraseasonal oscillation: Convective momentum transport. *Geophysical Research Letters*, *37*, L24804. https://doi.org/10.1029/2010GL045072

Katsumata, M., Ciesielski, P. E., & Johnson, R. H. (2011). Evaluation of budget analysis during MISMO. *Journal of Applied Meteorological Climatology*, *50*, 241–254. https://doi.org/10.1175/2010jamc2515.1

Kemball-Cook, S. R., & Weare, B. C. (2001). The onset of convection in the madden-Julian oscillation. *Journal of Climate*, *14*(5), 780–793. https://doi.org/10.1175/1520-0442(2001)014<0780:TOOCIT>2.0.CO;2

Kikuchi, K., Wang, B., & Fudeyasu, H. (2009). Genesis of tropical cyclone Nargis revealed by multiple satellite observations. *Geophysical Research Letters*, *36*, L06811. https://doi.org/10.1029/2009GL037296

Lee, J.-Y., Kwon, M., Yun, K.-S., Min, S.-K., Park, I. H., Ham, Y. G., et al. (2017). The long-term variability of Changma in the east Asian summer monsoon system: A review and revisit. *Asia-Pacific Journal of Atmospheric Sciences*, *53*(2), 257–272. https://doi.org/10.1007/s13143-017-0032-5

Lee, J.-Y., Wang, B., Seo, K.-H., Ha, K.-J., Kitoh, A., & Liu, J. (2015). Effects of mountain uplift on global monsoon precipitation. *Asia-Pacific Journal of Atmospheric Sciences*, *51*, 275–290. https://doi.org/10.1007/s13143-015-0077-2

Lee, J. Y., Wang, B., Wheeler, M. C., Fu, X., Waliser, D. E., & Kang, I.-S. (2013). Real-time multivariate indices for the boreal summer intraseasonal oscillation over the Asian summer monsoon region. *Climate Dynamics*, *40*, 493–509. https://doi.org/10.1007/s00382-012-1544-4

Li, K., Li, Z., Yang, Y., Xiang, B., Liu, Y., & Yu, W. (2015). Strong modulations on the bay of Bengal monsoon onset vortex by the first northward-propagating intra-seasonal oscillation. *Climate Dynamics*, *47*, 107–115. https://doi.org/10.1007/s00382-015-2826-4

Liu, F., Wang, B., & Kang, I.-S. (2015). Role of barotropic convective momentum transport in the intraseasonal oscillation. *Journal of Climate*, *28*, 4908–4920. https://doi.org/10.1175/JCLI-D-14-00575.1

Liu, F., Zhao, J., Fu, X., & Huang, G. (2018). The role of shallow convection in promoting the northward propagation of boreal summer intraseasonal oscillation. *Theoretical Applied Climatology*, *131*(3–4), 1387–1395. https://doi.org/10.1007/s00704-017-2064-2

Maloney, E. D., & Hartmann, D. L. (2001). The Madden-Julian Oscillation, barotropic dynamics, and North Pacific tropical cyclone formation. Part I: Observations. *Journal of the Atmospheric Sciences*, *58*, 2545–2558. https://doi.org/10.1175/1520-0469(2001)058<2545:TMJOBD>2.0.CO;2

Moon, J.-Y., Wang, B., Ha, K.-J., & Lee, J.-Y. (2013). Teleconnections associated with Northern Hemisphere summer monsoon intraseasonal oscillation. *Climate Dynamics*, *40*, 2761–2774. https://doi.org/10.1007/s00382-012-1394-0

Moon, J. Y., Wang, B., Lee, S.-S., & Ha, K.-J. (2018). An intraseasonal genesis potential index for tropical cyclones during northern hemisphere summer. *Journal of Climate*, *31*(22), 9055–9071. https://doi.org/10.1175/JCLI-D-18-0515.1

Simmons, A., Uppala, S., Dee, D., & Kobayashi, S. (2007). ERA-Interim: newECMWF reanalysis products from 1989 onwards. *ECMWF News*, *110*, 25–35.

Stephens, G. L., Vane, D. G., Boain, R. J., Mace, G. G., Sassen, K., Wang, Z., et al. (2002). The cloudsat mission and the a-train. *Bulletin of the American Meteorological Society*, *83*(12), 1771–1790. https://doi.org/10.1175/bams-83-12-1771

Tiedtke, M., Heckley, W. A., & Slingo, J. (1988). Tropical forecasting at ECMWF: On the influence of physical parametrization on the mean structure of forecasts and analyses. *Quarterly Journal of the Royal Meteorological Society*, *114*, 639–664.

Wang, B., & Rui, H. (1990). Dynamics of the coupled moist kelvin-Rossby wave on an equatorial β-plane. *Journal of the Atmospheric Sciences*, *47*(4), 397–413. https://doi.org/10.1175/1520-0469(1990)047<0397:DOTCMK>2.0.CO;2

Wang, B., & Xie, X. (1996). Low-frequency equatorial waves in vertically sheared zonal flow. Part I: Stable waves. *Journal of the Atmospheric Sciences*, *53*, 449–467. https://doi.org/10.1175/1520-0469(1996)053<0449:LFEWIV>2.0.CO;2

Wang, B., & Xie, X. (1997). A model for the boreal summer intraseasonal oscillation. *Journal of the Atmospheric Sciences*, *54*, 72–86. https://doi.org/10.1175/1520-0469(1997)054<0072:AMFTBS>2.0.CO;2

Xie, X., & Wang, B. (1996). Low-frequency equatorial waves in vertically sheared zonal flow. Part II: Unstable waves. *Journal of the Atmospheric Sciences*, *53*, 3589–3605. https://doi.org/10.1175/1520-0469(1996)053<3589:LFEWIV>2.0.CO;2

Yang, J., Wang, B., & Bao, Q. (2010). Biweekly and 21-30-day variations of the subtropical summer monsoon rainfall over the lower reach of the Yangtze River basin. *Journal of Climate*, *23*, 1146–1159. https://doi.org/10.1175/2009JCLI3005.1

Yang, Y.-M., An, S.-I., Wang, B., & Park, J. H. (2020). A global-scale multidecadal variability driven by Atlantic multidecadal oscillation. *National Science Review*, *7*, nwz216. https://doi.org/10.1093/nsr/nwz216

Yang, Y.-M., Lee, J.-Y., & Wang, B. (2019). The Tibetan plateau uplift is crucial for eastward propagation of Madden–Julian Oscillation. *Scientific Reports*, *9*, 15478. https://doi.org/10.1038/s41598-019-56013-w

Yang, Y.-M., & Wang, B. (2019). Improving MJO simulation by enhancing the interaction between boundary layer convergence and lower tropospheric heating. *Climate Dynamics*, *52*, 4671–4693. https://doi.org/10.1007/s00382-018-4407-9

Yang, Y.-M., Wang, B., Cao, J., Ma, L., & Li, J. (2020). Improved historical simulation by enhancing moist physical parameterizations in the climate system model NESM3. *0. Climate Dynamics*, *54*(7–8), 3819–3840. https://doi.org/10.1007/s00382-020-05209-2

Yang, Y.-M., Wang, B., & Lee, J.-Y. (2019). Mechanisms of northward propagation of boreal summer intraseasonal oscillation revealed by climate model experiments. *Geophysical Research Letters*, *46*, 3417–3425. https://doi.org/10.1029/2018GL081612

Yang, Y. M., Wang, B., & Li, J. (2018). Improving seasonal prediction of east Asian summer rainfall using NESM3.0: Preliminary results. *Atmosphere*, *9*, 487. https://doi.org/10.3390/atmos9120487

Zheng, Y., Waliser, D. E., Stern, W., & Jones, C. (2004). The role of coupled sea surface temperatures in the simulation of the tropical intraseasonal oscillation. *Journal of Climate*, *17*, 4109–4134. https://doi.org/10.1175/JCLI3202.1

Zhu, B., & Wang, B. (1993). The 30–60-day convection seesaw between the tropical Indian and western Pacific oceans. *Journal of the Atmospheric Sciences*, *50*, 184–199. https://doi.org/10.1175/1520-0469(1993)050<0184:TDCSBT>2.0.CO;2